THE ASTROPHYSICAL JOURNAL, 197:379–391, 1975 April 15

ULTRAVIOLET PHOTOMETRY FROM THE ORBITING ASTRONOMICAL OBSERVATORY. XIX. ATMOSPHERIC PROPERTIES OF THE DETACHED BINARIES VV ORIONIS AND MR CYGNI

JOEL A. EATON
Washburn Observatory, University of Wisconsin, Madison
Received 1974 September 9; revised 1974 November 4

ABSTRACT

A series of OAO 2 light curves for VV Ori covering the wavelength range 1300–4300 Å is presented. Analysis of these light curves using light-curve synthesis techniques leads to a mass ratio for the system consistent with radial-velocity observations and to limb darkening consistent with theory. The gravity darkening for the primary, however, is *much less* ($g = 0.3$) than theoretically expected for stars with radiative envelopes. Analysis of light curves for MR Cyg, a system similar to VV Ori, indicates that the gravity darkening of MR Cyg *could be* as low as that found for VV Ori. The mass-luminosity relation applied to this system, however, implies that the primary is probably fully gravity darkened or that the stars may not be adequately represented by Roche potentials. For both of these systems the wavelength dependence of the reflection effect is qualitatively that which is expected from the predictions of Rucinski, although for VV Ori it is higher than expected in the ultraviolet.

Subject headings: eclipsing binaries — early-type stars — stars, individual — ultraviolet

I. INTRODUCTION

The purpose of this study is to determine certain atmospheric properties, namely limb and gravity darkening, for an early B star by solving a set of simultaneous ultraviolet light curves for VV Orionis. The light curves of VV Ori are particularly well suited for determining limb and gravity darkening. Hopefully, the values determined for these quantities should apply to other stars of similar temperature and gravity. The highly analyzed system MR Cygni offers a chance to test this applicability; here, it will be analyzed once again with particular emphasis given to the range of limb and gravity darkening consistent with its light curves.

VV Orionis is an eclipsing binary of early spectral type (B1 + middle B) in the belt region of Orion. From the standpoint of determining limb and gravity darkening for B stars it is an extremely important system. Primary eclipse is a complete transit with a reasonably long duration of the complete phases. The out-of-eclipse distortion of the light curve is moderate, although probably low enough to rectify satisfactorily in a Russell-model analysis. Spectroscopically, only the primary is visible, although blending of the lines of the secondary is detectable near the quadratures.

The most extensive early photoelectric work on this system was carried out by Huffer using a 15-inch (38 cm) refractor and an unfiltered 1P21 photocell (Huffer and Kopal 1951). Huffer later obtained a two-color light curve using a reflector (Huffer and Kopal 1952). To my knowledge, neither his later observations nor their complete solution was ever published; however, I have been able to examine Huffer's original plots of them. These plots show rather poor out-of-eclipse coverage with primary eclipse shallower by about 0.03 mag in both blue and yellow light than was the primary in the earlier Huffer light curve. These unpublished curves have eclipse depths similar to the 4250 Å satellite (OAO 2) light curve to be presented here, while the refractor light curve agrees better with the observations of Wood (1946). E. W. Weis (unpublished) has obtained partial *uvby* light curves for the system which have depths similar to the blue OAO 2 light curve.

Early spectroscopic work on VV Ori was carried out by Daniel (1915) and by Struve and Luyten (1949). More recently, Beltrami and Galeotti (1970) have done a somewhat more detailed analysis, deriving a velocity amplitude for the secondary from the line shapes near quadrature. This analysis leads to a mass ratio of 0.44, which although fairly uncertain leads to a mass of the primary consistent with its spectral type. All three of these studies found essentially the same velocity amplitude for the primary.

MR Cygni is a system somewhat similar to VV Ori. It has a slightly later primary (B3 as opposed to B1) and more out-of-eclipse light variation. Primary eclipse is a very deep partial transit in the previous analyses. Hardie has obtained *UBV* light curves for this system (Hall and Hardie 1969); coverage of the eclipses is excellent in this work, although many of the out-of-eclipse observations were made at the beginning or at the end of eclipse observing sessions.

The radial velocity observations of MR Cyg are contradictory. Pearce (Harper *et al.* 1935) observed a velocity amplitude for the primary of $K_1 = 173$ km s^{-1}. Wilson and Devinney (1971) have rediscussed Pearce's work, looking particularly at the radial velocities of the secondary. Although they were apparently unable to detect the lines of the secondary in the selected spectrograms they saw, nonetheless they found a mass ratio of 0.83 from Pearce's unpublished radial velocity measurements. Later observations by Hill and Hutchings (1973), at reasonably

TABLE 1

OAO - 2 PHOTOMETRY OF VV ORIONIS

Observations for λ4250 Å

$JD_{\odot}$ 2440000+	Phase	Intensity	$JD_{\odot}$	Phase	Intensity	$JD_{\odot}$	Phase	Intensity	$JD_{\odot}$	Phase	Intensity	$JD_{\odot}$	Phase	Intensity
492.2094	0.8467	0.971	840.3485	0.2240	0.995	847.2410	0.8642	0.966	849.1204	0.1295	0.974	850.8624	0.3023	0.991
492.2101	0.8472	0.976	840.3507	0.2255	0.995	847.2433	0.8658	0.966	849.1228	0.1311	0.970	850.9295	0.3475	0.983
492.2787	0.8934	0.963	840.4181	0.2709	0.995	847.3140	0.9134	0.953	849.1900	0.1764	0.987	850.9319	0.3491	0.987
492.2797	0.8940	0.959	840.4203	0.2723	0.991	847.3163	0.9150	0.949	849.1923	0.1780	0.991	851.0025	0.3966	0.978
492.3483	0.9402	0.868	840.4878	0.3178	0.987	847.3859	0.9618	0.779	849.2635	0.2258	0.991	851.0049	0.3982	0.978
492.3492	0.9408	0.860	840.4900	0.3193	0.991	847.7283	0.1923	1.004	849.2659	0.2275	0.995	851.0695	0.4417	0.915
492.4178	0.9870	0.744	840.6966	0.4584	0.885	847.7971	0.2387	1.000	849.3336	0.2731	1.004	851.0719	0.4433	0.910
492.4187	0.9876	0.744	840.7664	0.5053	0.864	847.7995	0.2403	0.995	849.3360	0.2746	0.991	851.1436	0.4916	0.876
495.8300	0.2842	1.004	840.7685	0.5068	0.872	847.8676	0.2861	0.991	849.4024	0.3194	0.995	851.1460	0.4932	0.881
495.8306	0.2846	1.004	840.8359	0.5521	0.910	847.8700	0.2877	1.004	849.4048	0.3210	0.987	851.2086	0.5353	0.876
495.9004	0.3316	0.992	840.8381	0.5536	0.910	847.9371	0.3329	0.987	849.7466	0.5511	0.872	851.2110	0.5369	0.881
495.9690	0.3778	0.984	840.9056	0.5991	0.978	847.9395	0.3345	0.978	849.7486	0.5524	0.919	851.2830	0.5855	0.978
495.9699	0.3784	0.980	840.9078	0.6006	0.974	848.0067	0.3797	0.978	849.8167	0.5983	0.983	851.2854	0.5871	0.970
496.7347	0.8933	0.951	841.3930	0.9272	0.915	848.0090	0.3813	0.987	849.8190	0.5998	0.987	851.3533	0.6328	0.991
496.8044	0.9402	0.868	841.3952	0.9287	0.898	848.0764	0.4267	0.957	849.8862	0.6451	0.983	851.3557	0.6344	0.983
496.8053	0.9408	0.864	841.4625	0.9740	0.749	848.0788	0.4282	0.953	849.8886	0.6467	0.983	851.4227	0.6795	0.987
496.8739	0.9870	0.741	841.4647	0.9755	0.745	848.1459	0.4735	0.876	849.9557	0.6919	1.000	851.4250	0.6811	0.991
496.8748	0.9876	0.741	841.7410	0.1615	0.983	848.1483	0.4751	0.864	849.9581	0.6935	0.991	851.6936	0.8619	0.978
496.9435	0.0338	0.753	841.8108	0.2085	0.995	848.2155	0.5203	0.881	850.0255	0.7388	1.000	851.7637	0.9091	0.953
496.9444	0.0344	0.778	841.8130	0.2099	0.995	848.2178	0.5219	0.872	850.0278	0.7404	1.000	851.7668	0.9111	0.953
497.0920	0.1338	0.967	841.8803	0.2553	1.000	848.2852	0.5672	0.953	850.0950	0.7856	0.983	851.8343	0.9566	0.796
497.0929	0.1344	0.963	841.8825	0.2567	1.008	848.2882	0.5693	0.944	850.0974	0.7872	0.991	851.8367	0.9582	0.783
497.1625	0.1813	1.009	841.9500	0.3022	0.991	848.3593	0.6171	0.983	850.1645	0.8325	0.987	851.9041	0.0036	0.745
497.2229	0.2219	0.996	841.9522	0.3037	0.991	848.3616	0.6187	0.991	850.1669	0.8340	0.974	851.9064	0.0052	0.745
839.3739	0.5679	0.944	842.0196	0.3490	0.983	848.7029	0.8484	0.966	850.2342	0.8794	0.961	851.9769	0.0526	0.851
839.3758	0.5692	0.949	842.0217	0.3505	0.995	848.7718	0.8949	0.970	850.2366	0.8810	0.966	851.9792	0.0542	0.851
839.7219	0.8022	0.995	842.0913	0.3973	0.978	848.7742	0.8965	0.974	850.3080	0.9290	0.902	852.0444	0.0980	0.953
839.7914	0.8490	0.966	842.1588	0.4428	0.919	848.8421	0.9422	0.860	850.3103	0.9306	0.902	852.0468	0.0996	0.957
839.7936	0.8505	0.978	842.1610	0.4442	0.919	848.8445	0.9438	0.855	850.3782	0.9763	0.753	852.2582	0.2420	0.991
839.8610	0.8958	0.961	842.2284	0.4896	0.876	848.9140	0.9905	0.753	850.3806	0.9779	0.749	852.2606	0.2436	0.991
839.8632	0.8973	0.957	842.2305	0.4911	0.868	848.9166	0.9923	0.741	850.4483	0.0235	0.749	852.3277	0.2888	0.995
839.9300	0.9423	0.860	842.3032	0.5400	0.893	848.9812	0.0358	0.775	850.7207	0.2069	0.991	852.3301	0.2904	1.000
839.9322	0.9437	0.851	842.3054	0.5414	0.902	848.9836	0.0374	0.792	850.7894	0.2531	1.008	852.3978	0.3360	0.987
840.2788	0.1771	0.991	847.1714	0.8174	0.978	849.0511	0.0828	0.944	850.7923	0.2551	1.004	852.4002	0.3376	0.995
840.2810	0.1786	0.987	847.1738	0.8190	0.983	849.0534	0.0844	0.953	850.8600	0.3007	0.995	852.7383	0.5652	0.932
852.7414	0.5673	0.949	852.8089	0.6127	0.978	852.8113	0.6143	0.983	852.8785	0.6596	0.991	852.8809	0.6612	0.991

Observations for λ3320 Å

$JD_{\odot}$ 2440000+	Phase	Intensity	$JD_{\odot}$	Phase	Intensity	$JD_{\odot}$	Phase	Intensity	$JD_{\odot}$	Phase	Intensity	$JD_{\odot}$	Phase	Intensity
491.6507	0.4706	0.889	493.1206	0.4601	0.894	497.2207	0.2205	1.003	841.9535	0.3045	0.984	848.2169	0.5212	0.878
491.6510	0.4708	0.895	493.1823	0.5017	0.879	839.3749	0.5686	0.941	842.0208	0.3499	0.975	848.2191	0.5227	0.871
491.7897	0.5642	0.942	493.1825	0.5019	0.883	839.3770	0.5700	0.942	842.0230	0.3514	0.975	848.2866	0.5682	0.948
491.7901	0.5644	0.957	493.2515	0.5483	0.911	839.7231	0.8030	0.982	842.0903	0.3967	0.967	848.2888	0.5697	0.945
491.9290	0.6579	0.995	493.2518	0.5485	0.900	839.7927	0.8498	0.960	842.0926	0.3982	0.970	848.3607	0.6181	0.970
491.9294	0.6582	0.998	493.3212	0.5952	0.978	839.7949	0.8513	0.964	842.1601	0.4436	0.914	848.3629	0.6195	0.977
492.1378	0.7985	0.995	493.3215	0.5954	0.977	839.8622	0.8966	0.939	842.1623	0.4451	0.911	848.7733	0.8958	0.949
492.1382	0.7988	0.998	493.3909	0.6421	0.987	839.8644	0.8981	0.946	842.2296	0.4904	0.875	848.7755	0.8973	0.947
492.2075	0.8455	0.981	493.3913	0.6424	0.984	839.9312	0.9431	0.830	842.2318	0.4919	0.875	848.8435	0.9431	0.837
492.2079	0.8457	0.981	495.8281	0.2829	1.003	839.9334	0.9446	0.824	842.3044	0.5408	0.893	848.8457	0.9446	0.823
492.2771	0.8923	0.963	495.8284	0.2832	0.994	840.2800	0.1779	0.973	842.3066	0.5423	0.896	848.9156	0.9917	0.708
492.2774	0.8925	0.961	495.8978	0.3299	0.997	840.2822	0.1794	0.972	847.1729	0.8184	0.969	848.9178	0.9931	0.712
492.3466	0.9391	0.865	495.8982	0.3301	0.997	840.3497	0.2248	0.990	847.1750	0.8198	0.972	848.9826	0.0368	0.754
492.3470	0.9393	0.863	495.9673	0.3767	0.986	840.3519	0.2263	0.995	847.2424	0.8652	0.947	848.9848	0.0382	0.771
492.4161	0.9859	0.732	495.9677	0.3769	0.986	840.4193	0.2717	0.990	847.2446	0.8667	0.957	849.0525	0.0838	0.928
492.4165	0.9861	0.729	496.1066	0.4704	0.876	840.4215	0.2731	1.002	847.3154	0.9143	0.922	849.0547	0.0853	0.939
492.4860	0.0330	0.744	496.1070	0.4707	0.886	840.6979	0.4592	0.911	847.3176	0.9158	0.928	849.1219	0.1305	0.961
492.4864	0.0332	0.748	496.1761	0.5172	0.876	840.7676	0.5062	0.869	847.3871	0.9626	0.744	849.1242	0.1321	0.964
492.5640	0.0855	0.939	496.1765	0.5175	0.888	840.8371	0.5530	0.906	847.7986	0.2396	0.984	849.1914	0.1773	0.964
492.5644	0.0857	0.944	496.8028	0.9391	0.860	840.8393	0.5545	0.907	847.8008	0.2411	0.996	849.1936	0.1788	0.976
492.6250	0.1265	0.967	496.8031	0.9393	0.867	840.9069	0.5999	0.981	847.8690	0.2871	0.996	849.2649	0.2268	0.997
492.6254	0.1268	0.979	496.8723	0.9859	0.723	840.9090	0.6014	0.976	847.8712	0.2885	1.003	849.2671	0.2283	0.991
492.7033	0.1792	0.991	496.8727	0.9862	0.722	841.3941	0.9280	0.899	847.9386	0.3339	0.978	849.3350	0.2740	0.997
492.7730	0.2262	0.998	496.9418	0.0327	0.737	841.3963	0.9295	0.896	847.9407	0.3353	0.987	849.3372	0.2755	0.996
492.7734	0.2264	1.000	496.9422	0.0330	0.736	841.7423	0.1624	0.970	848.0081	0.3807	0.975	849.4060	0.3218	0.994
492.9034	0.3140	0.993	497.0904	0.1327	0.958	841.8121	0.2093	0.991	848.0103	0.3822	0.977	849.7476	0.5518	0.922
492.9038	0.3142	0.995	497.0907	0.1330	0.965	841.8142	0.2108	0.982	848.0778	0.4276	0.945	849.8181	0.5992	0.975
493.0427	0.4077	0.982	497.1599	0.1795	0.981	841.8815	0.2561	1.000	848.0800	0.4291	0.948	849.8203	0.6007	0.975
493.0430	0.4080	0.976	497.1603	0.1798	0.994	841.8837	0.2576	1.001	848.1473	0.4744	0.876	849.8876	0.6460	0.970
493.1202	0.4599	0.896	497.2203	0.2202	1.011	841.9513	0.3030	0.995	848.1495	0.4759	0.872	849.8898	0.6475	0.987

TABLE 1 - Continued

Observations for λ3320 Å, Continued

JD$_\odot$ 2440000+	Phase	Intensity
849.9572	0.6928	0.994
849.9593	0.6943	0.991
850.0269	0.7398	1.001
850.0291	0.7413	1.008
850.0964	0.7866	0.978
850.0986	0.7881	0.993
850.1660	0.8334	0.984
850.1681	0.8349	0.977
850.2357	0.8803	0.954
850.2379	0.8818	0.957
852.4014	0.3384	0.982
850.3094	0.9300	0.889
850.3116	0.9315	0.884
850.3797	0.9773	0.724
850.3818	0.9788	0.728
850.4519	0.0259	0.728
850.7913	0.2544	0.991
850.7935	0.2559	1.001
850.8614	0.3016	0.996
850.8636	0.3031	0.989
850.9310	0.3484	0.988
852.7405	0.5666	0.946
850.9331	0.3499	0.994
851.0040	0.3976	0.976
851.0061	0.3991	0.983
851.0709	0.4427	0.911
851.0731	0.4442	0.920
851.1450	0.4926	0.884
851.1472	0.4940	0.882
851.2100	0.5363	0.888
851.2122	0.5378	0.883
851.2845	0.5864	0.969
852.8104	0.6137	0.976
851.2867	0.5879	0.975
851.3547	0.6337	0.999
851.3569	0.6352	0.987
851.4241	0.6804	0.982
851.4263	0.6819	0.997
851.7659	0.9105	0.935
851.7680	0.9120	0.936
851.8358	0.9576	0.767
851.8378	0.9590	0.768
851.9055	0.0045	0.721
852.8125	0.6152	0.972
852.8799	0.6605	0.987
851.9077	0.0060	0.715
851.9783	0.0535	0.839
851.9805	0.0550	0.841
852.0458	0.0990	0.953
852.0480	0.1005	0.949
852.2596	0.2429	0.994
852.2618	0.2444	0.996
852.3292	0.2898	0.997
852.3313	0.2912	1.005
852.3992	0.3369	0.975
852.8821	0.6620	0.999

Observations for λ2980 Å

JD$_\odot$ 2440000+	Phase	Intensity
491.6538	0.4727	0.885
491.6547	0.4733	0.895
491.7929	0.5663	0.951
491.7938	0.5669	0.948
491.9322	0.6601	0.982
491.9331	0.6607	0.993
492.0712	0.7537	1.007
492.0721	0.7543	1.000
492.1410	0.8006	0.992
492.1419	0.8013	1.003
492.2107	0.8476	0.983
492.2802	0.8944	0.962
492.2811	0.8950	0.952
492.3497	0.9412	0.860
492.3507	0.9418	0.851
492.4193	0.9880	0.727
492.4202	0.9886	0.722
492.4892	0.0351	0.754
492.4901	0.0357	0.757
492.5672	0.0876	0.942
492.5681	0.0882	0.939
492.6282	0.1286	0.969
492.6291	0.1293	0.971
492.7061	0.1811	0.981
492.7070	0.1817	0.974
492.7762	0.2283	1.003
492.7771	0.2289	0.997
492.9066	0.3161	0.990
492.9075	0.3167	0.994
493.0458	0.4098	0.974
493.0467	0.4104	0.964
493.1234	0.4620	0.879
493.1243	0.4626	0.878
493.1851	0.5036	0.889
493.1860	0.5042	0.892
493.2546	0.5504	0.906
493.2555	0.5510	0.912
493.3243	0.5973	0.960
493.3252	0.5979	0.978
495.8312	0.2850	1.005
852.7394	0.5659	0.946
495.8321	0.2857	1.000
495.9010	0.3320	1.003
495.9019	0.3326	1.002
495.9705	0.3788	0.984
495.9714	0.3794	0.986
496.1107	0.4732	0.888
496.1793	0.5194	0.879
496.1802	0.5200	0.884
496.8059	0.9412	0.846
496.8068	0.9418	0.846
496.8755	0.9880	0.718
496.8764	0.9887	0.719
496.9450	0.0349	0.738
496.9459	0.0355	0.739
497.0935	0.1349	0.956
497.0944	0.1355	0.956
497.1631	0.1817	0.975
497.1640	0.1823	0.964
497.2235	0.2224	0.994
497.2244	0.2230	0.995
839.7222	0.8024	0.996
839.7918	0.8492	0.968
839.7940	0.8507	0.969
839.8613	0.8960	0.947
839.8635	0.8975	0.948
839.9303	0.9425	0.834
839.9325	0.9440	0.825
840.2791	0.1773	0.980
840.2809	0.1785	0.984
840.3350	0.2150	1.012
840.3488	0.2242	0.999
840.3510	0.2257	1.002
840.4206	0.2725	0.988
840.6970	0.4586	0.894
840.7667	0.5056	0.890
840.7689	0.5070	0.885
840.8362	0.5524	0.915
840.8384	0.5538	0.916
840.9059	0.5993	0.982
840.9081	0.6008	0.974
852.7417	0.5675	0.953
841.3932	0.9274	0.891
841.3954	0.9288	0.902
841.7414	0.1617	0.977
841.8111	0.2087	0.989
841.8133	0.2101	0.994
841.8806	0.2555	1.005
841.8828	0.2570	1.007
841.9503	0.3024	1.000
841.9525	0.3039	0.998
842.0199	0.3493	0.982
842.0221	0.3507	0.984
842.0894	0.3961	0.987
842.0916	0.3975	0.977
842.1591	0.4430	0.923
842.1613	0.4445	0.925
842.2287	0.4898	0.883
842.2309	0.4913	0.885
842.3035	0.5402	0.898
842.3057	0.5417	0.898
847.1718	0.8176	0.975
847.1741	0.8192	0.977
847.2413	0.8645	0.959
847.2437	0.8660	0.964
847.3143	0.9136	0.934
847.3167	0.9152	0.938
847.3862	0.9620	0.761
847.7975	0.2389	0.996
847.7998	0.2405	0.994
847.8679	0.2863	0.993
847.8703	0.2879	1.017
847.9375	0.3331	0.989
847.9398	0.3347	0.984
848.0070	0.3799	0.975
848.0094	0.3815	0.968
848.0768	0.4269	0.951
848.0791	0.4285	0.953
848.1463	0.4737	0.883
848.1486	0.4753	0.880
848.2158	0.5205	0.883
848.2182	0.5221	0.901
852.8093	0.6130	0.988
848.2855	0.5674	0.947
848.2879	0.5690	0.947
848.3596	0.6173	0.984
848.3620	0.6189	0.975
848.7722	0.8951	0.954
848.7745	0.8967	0.953
848.8425	0.9424	0.842
848.8448	0.9440	0.843
848.9145	0.9909	0.717
848.9169	0.9925	0.713
848.9815	0.0360	0.754
848.9839	0.0376	0.756
849.0514	0.0831	0.932
849.0538	0.0847	0.939
849.1208	0.1298	0.954
849.1231	0.1314	0.965
849.1903	0.1766	0.974
849.1927	0.1782	1.000
849.2639	0.2261	1.013
849.2662	0.2277	0.997
849.3339	0.2733	1.002
849.3363	0.2749	0.998
849.4051	0.3212	0.996
849.7465	0.5510	0.917
849.8170	0.5985	0.970
849.8193	0.6001	0.972
849.8865	0.6453	0.987
849.8889	0.6469	0.974
849.9561	0.6921	0.992
849.9584	0.6937	0.987
850.0258	0.7390	0.993
850.0282	0.7406	0.992
850.0953	0.7859	0.992
850.0977	0.7875	0.992
850.1649	0.8327	0.978
850.1672	0.8343	0.978
850.2346	0.8796	0.967
850.2369	0.8812	0.958
850.3083	0.9292	0.891
850.3107	0.9308	0.881
852.8116	0.6146	0.985
852.8788	0.6598	0.998
850.3786	0.9766	0.723
850.3809	0.9781	0.724
850.4510	0.0253	0.725
850.7211	0.2071	1.009
850.7902	0.2537	1.015
850.7926	0.2553	1.002
850.8603	0.3009	1.003
850.8627	0.3025	1.000
850.9299	0.3477	0.984
850.9322	0.3493	0.995
851.0029	0.3968	0.980
851.0052	0.3984	0.974
851.0698	0.4419	0.917
851.0722	0.4435	0.912
851.1439	0.4918	0.884
851.1463	0.4934	0.886
851.2090	0.5356	0.917
851.2113	0.5372	0.907
851.2834	0.5857	0.982
851.2857	0.5873	0.978
851.3536	0.6330	0.992
851.3560	0.6346	0.978
851.4230	0.6797	0.997
851.4254	0.6813	0.985
851.7648	0.9098	0.947
851.7671	0.9114	0.945
851.8347	0.9568	0.764
851.8370	0.9584	0.754
851.9044	0.0038	0.709
851.9068	0.0054	0.717
851.9772	0.0528	0.830
851.9796	0.0544	0.829
852.0447	0.0983	0.943
852.0471	0.0999	0.935
852.2585	0.2422	1.000
852.2609	0.2438	1.000
852.3281	0.2890	1.003
852.3304	0.2906	0.999
852.3981	0.3362	0.990
852.4005	0.3378	0.992
852.8812	0.6614	1.005

Observations for λ2460 Å

JD$_\odot$ 2440000+	Phase	Intensity
491.6532	0.4723	0.890
491.7923	0.5659	0.936
491.9316	0.6597	0.975
492.0706	0.7533	0.991
492.1403	0.8002	0.991
492.2101	0.8472	0.969
492.2796	0.8940	0.951
492.3491	0.9408	0.847
492.4187	0.9876	0.706
492.4886	0.0347	0.737
492.5666	0.0872	0.951
492.6276	0.1282	0.963
492.7055	0.1807	0.994
492.7756	0.2279	1.006
492.9060	0.3157	0.994
493.0452	0.4094	0.975
493.1228	0.4616	0.905
493.1845	0.5032	0.899
493.2540	0.5500	0.914
493.3237	0.5969	0.978
495.8306	0.2846	0.988
495.9004	0.3316	0.985
495.9699	0.3784	0.969
496.1091	0.4721	0.890
496.1787	0.5189	0.881
496.8053	0.9408	0.850
496.8748	0.9876	0.713
496.9444	0.0344	0.740
497.0929	0.1344	0.975
497.1625	0.1813	1.000
497.2229	0.2219	1.003
839.3761	0.5694	0.944
839.3771	0.5700	0.948
839.4459	0.6163	0.970
839.4468	0.6170	0.966
839.7244	0.8039	0.992
839.7254	0.8045	0.998
839.7940	0.8507	0.966
839.7949	0.8513	0.966
839.8635	0.8975	0.948
839.8645	0.8981	0.954
839.9325	0.9440	0.833
839.9334	0.9446	0.830
840.2813	0.1788	0.986
840.2822	0.1794	0.993
840.3510	0.2257	1.009
840.3520	0.2263	1.009
840.4206	0.2725	0.990
840.4215	0.2732	1.009
840.6991	0.4601	0.910
840.7689	0.5070	0.878
840.8384	0.5538	0.904
840.8394	0.5545	0.916
840.9081	0.6008	0.968
840.9091	0.6014	0.970
841.3954	0.9288	0.885
841.3964	0.9295	0.885
841.4659	0.9763	0.718
841.7445	0.1638	0.982
841.8133	0.2101	0.982
841.8142	0.2108	0.992
841.8828	0.2570	0.995
841.8838	0.2576	1.001
841.9525	0.3039	0.992
841.9535	0.3045	0.995
842.0221	0.3507	0.976
842.0230	0.3514	0.982
842.0916	0.3975	0.966
842.0926	0.3982	0.973
842.1613	0.4445	0.907
842.1623	0.4451	0.913
842.2309	0.4913	0.872
842.2318	0.4919	0.888
842.3057	0.5417	0.897
842.3066	0.5423	0.904

TABLE 1 - Continued

Observations for λ2460 Å, Continued

$JD_\odot$	Phase	Intensity	$JD_\odot$	Phase	Intensity	$JD_\odot$	Phase	Intensity	$JD_\odot$	Phase	Intensity	$JD_\odot$	Phase	Intensity
2440000+														
847.1746	0.8195	0.986	848.2879	0.5690	0.938	849.3373	0.2755	0.997	850.3116	0.9315	0.885	851.2867	0.5879	0.970
847.1751	0.8199	0.986	848.2883	0.5694	0.951	849.4056	0.3215	0.997	850.3814	0.9785	0.715	851.3565	0.6349	0.989
847.2437	0.8660	0.967	848.2888	0.5697	0.951	849.4061	0.3218	0.997	850.3819	0.9788	0.718	851.3570	0.6352	0.989
847.2446	0.8667	0.967	848.3620	0.6189	0.977	849.7493	0.5529	0.910	850.4520	0.0260	0.718	851.4266	0.6821	0.995
847.3167	0.9152	0.935	848.3629	0.6196	0.980	849.7498	0.5533	0.904	850.7244	0.2094	0.998	851.4272	0.6825	0.998
847.3176	0.9158	0.935	848.8453	0.9443	0.828	849.8198	0.6004	0.979	850.7931	0.2556	1.004	851.7676	0.9117	0.944
847.3862	0.9620	0.738	848.8458	0.9446	0.828	849.8203	0.6007	0.979	850.7936	0.2559	1.007	851.7681	0.9120	0.948
847.3872	0.9626	0.745	848.9169	0.9925	0.700	849.8893	0.6472	0.982	850.8631	0.3028	0.998	851.8375	0.9587	0.762
847.8703	0.2879	0.999	848.9179	0.9932	0.706	849.8898	0.6475	0.985	850.8636	0.3031	0.995	851.8380	0.9591	0.762
847.8712	0.2885	1.009	848.9839	0.0376	0.761	849.9589	0.6940	0.998	850.9327	0.3496	0.989	851.9072	0.0057	0.712
847.9398	0.3347	0.993	848.9849	0.0383	0.767	849.9594	0.6943	1.001	850.9332	0.3499	0.992	851.9077	0.0060	0.712
847.9408	0.3354	0.996	849.0538	0.0847	0.938	850.0287	0.7410	1.004	851.0057	0.3987	0.976	851.9800	0.0547	0.837
848.0094	0.3816	0.970	849.0547	0.0853	0.944	850.0291	0.7413	1.004	851.0062	0.3991	0.979	851.9805	0.0550	0.841
848.0103	0.3822	0.977	849.1236	0.1317	0.967	850.0982	0.7878	0.998	851.0734	0.4443	0.916	852.0476	0.1002	0.951
848.0791	0.4285	0.951	849.1243	0.1321	0.970	850.0986	0.7881	0.998	851.0739	0.4447	0.919	852.0480	0.1005	0.951
848.0800	0.4291	0.957	849.1932	0.1785	0.991	850.1677	0.8346	0.985	851.1467	0.4937	0.894	852.2614	0.2441	0.998
848.1486	0.4753	0.880	849.1936	0.1788	0.991	850.1682	0.8349	0.985	851.1472	0.4940	0.894	852.2619	0.2444	0.998
848.1496	0.4759	0.893	849.2667	0.2280	1.000	850.2374	0.8815	0.957	851.2117	0.5375	0.897	852.3309	0.2909	0.995
848.2182	0.5221	0.886	849.2672	0.2283	1.003	850.2379	0.8818	0.957	851.2122	0.5378	0.897	852.3314	0.2912	1.001
848.2191	0.5227	0.896	849.3368	0.2752	0.997	850.3111	0.9311	0.885	851.2862	0.5876	0.970	852.4010	0.3381	0.982
852.4015	0.3384	0.998	852.7427	0.5681	0.948				852.8126	0.6152	0.979	852.8816	0.6617	0.992
852.7422	0.5678	0.948	852.8121	0.6149	0.973							852.8821	0.6620	0.992

Observations for λ1920 Å

$JD_\odot$	Phase	Intensity	$JD_\odot$	Phase	Intensity	$JD_\odot$	Phase	Intensity	$JD_\odot$	Phase	Intensity	$JD_\odot$	Phase	Intensity
2440000+														
491.6510	0.4708	0.882	495.8284	0.2832	0.997	840.6988	0.4599	0.952	847.9386	0.3339	0.975	850.1676	0.8345	0.983
491.6516	0.4712	0.885	495.8290	0.2836	0.999	840.7681	0.5065	0.889	847.9390	0.3342	0.981	850.2361	0.8807	0.948
491.7901	0.5644	0.924	495.8982	0.3301	0.990	840.7685	0.5068	0.886	847.9399	0.3347	0.984	850.2366	0.8810	0.955
491.7907	0.5648	0.927	495.8988	0.3305	0.991	840.8376	0.5533	0.916	848.0086	0.3810	0.963	850.3099	0.9303	0.879
491.9294	0.6582	0.964	495.9677	0.3769	0.961	840.8381	0.5536	0.919	848.0090	0.3813	0.966	850.3103	0.9306	0.881
491.9300	0.6586	0.971	495.9683	0.3773	0.966	840.9073	0.6002	0.972	848.0783	0.4279	0.941	850.3801	0.9776	0.696
492.0690	0.7522	0.993	496.1070	0.4707	0.887	840.9078	0.6006	0.975	848.0788	0.4282	0.943	850.3806	0.9779	0.701
492.1388	0.7992	0.996	496.1076	0.4711	0.893	841.3946	0.9283	0.879	848.1478	0.4747	0.877	850.4507	0.0251	0.712
492.2079	0.8457	0.970	496.1765	0.5175	0.882	841.3951	0.9286	0.877	848.1483	0.4751	0.880	850.7918	0.2547	1.000
492.2085	0.8461	0.974	496.1771	0.5179	0.887	841.4641	0.9751	0.710	848.2173	0.5215	0.888	850.7923	0.2551	1.010
492.2774	0.8925	0.951	496.8031	0.9393	0.854	841.4646	0.9754	0.710	848.2345	0.5331	0.885	850.8619	0.3019	0.988
492.2780	0.8929	0.950	496.8037	0.9398	0.850	841.7432	0.1630	0.971	848.8440	0.9434	0.822	850.8624	0.3023	0.986
492.3470	0.9393	0.847	496.8727	0.9862	0.695	841.7427	0.1627	0.990	848.8445	0.9438	0.819	850.9312	0.3486	0.979
492.3476	0.9397	0.846	496.8733	0.9866	0.695	841.8125	0.2096	0.990	848.9161	0.9920	0.679	850.9317	0.3489	0.977
492.4165	0.9861	0.701	496.9422	0.0330	0.720	841.8130	0.2099	1.000	848.9166	0.9923	0.684	851.0044	0.3979	0.962
492.4171	0.9866	0.696	496.9428	0.0334	0.724	841.8820	0.2564	0.990	848.9831	0.0371	0.742	851.0049	0.3982	0.961
492.4864	0.0332	0.718	497.0907	0.1330	0.962	841.8825	0.2567	1.000	848.9836	0.0374	0.747	851.0714	0.4430	0.910
492.4870	0.0336	0.720	497.0913	0.1334	0.972	841.9517	0.3034	0.988	849.0530	0.0841	0.930	851.0719	0.4433	0.910
492.5644	0.0857	0.940	497.1603	0.1798	0.989	841.9522	0.3037	0.990	849.0535	0.0844	0.926	851.1455	0.4929	0.888
492.5650	0.0861	0.948	497.1609	0.1802	0.989	842.0213	0.3502	0.966	849.1223	0.1308	0.955	851.1460	0.4932	0.892
492.6254	0.1268	0.960	497.2207	0.2205	0.994	842.0217	0.3505	0.963	849.1228	0.1311	0.958	851.2105	0.5366	0.888
492.6260	0.1272	0.960	497.2213	0.2209	1.006	842.0908	0.3970	0.961	849.1919	0.1776	0.985	851.2110	0.5369	0.894
492.7033	0.1792	0.996	839.3749	0.5685	0.958	842.0913	0.3973	0.966	849.1924	0.1780	0.985	851.2849	0.5867	0.955
492.7039	0.1796	1.000	839.3753	0.5688	0.943	842.1605	0.4439	0.907	849.2654	0.2271	0.996	851.2854	0.5871	0.961
492.7734	0.2264	1.008	839.3758	0.5692	0.940	842.1610	0.4442	0.910	849.2659	0.2275	1.000	851.3552	0.6341	0.981
492.7740	0.2268	1.005	839.4446	0.6155	0.962	842.2300	0.4907	0.879	849.3355	0.2743	0.992	851.3557	0.6344	0.981
492.9038	0.3142	0.988	839.4455	0.6161	0.958	842.2305	0.4911	0.884	849.3360	0.2747	0.993	851.4246	0.6807	0.986
492.9044	0.3146	0.991	839.7241	0.8036	0.995	842.3049	0.5411	0.898	849.7481	0.5521	0.912	851.4250	0.6811	1.000
493.0430	0.4080	0.965	839.7931	0.8501	0.971	842.3054	0.5414	0.901	849.7486	0.5524	0.908	851.7663	0.9108	0.937
493.0436	0.4084	0.969	839.7936	0.8505	0.978	847.1733	0.8187	0.977	849.8185	0.5995	0.961	851.7668	0.9112	0.939
493.1206	0.4601	0.902	839.8627	0.8970	0.944	847.1738	0.8190	0.979	849.8190	0.5998	0.966	851.8362	0.9579	0.754
493.1212	0.4606	0.906	839.8634	0.8974	0.944	847.2429	0.8655	0.961	849.8881	0.6463	0.969	851.8367	0.9582	0.754
493.1823	0.5017	0.888	839.9317	0.9434	0.828	847.2433	0.8658	0.960	849.8886	0.6467	0.972	851.9059	0.0048	0.695
493.1829	0.5021	0.895	839.9322	0.9437	0.833	847.3159	0.9146	0.930	849.9576	0.6932	0.987	851.9064	0.0052	0.698
493.2518	0.5485	0.905	840.2805	0.1782	0.983	847.3163	0.9150	0.937	849.9581	0.6935	0.990	851.9788	0.0538	0.822
493.2524	0.5489	0.908	840.2810	0.1785	0.985	847.3854	0.9615	0.735	850.0273	0.7401	1.000	851.9792	0.0542	0.824
493.3215	0.5954	0.962	840.3502	0.2252	0.997	847.3859	0.9618	0.735	850.0278	0.7404	1.000	852.0463	0.0993	0.942
493.3222	0.5959	0.966	840.3507	0.2255	0.993	847.7307	0.1939	1.003	850.0969	0.7869	0.987	852.0468	0.0996	0.943
493.3913	0.6424	0.980	840.4202	0.2723	1.000	847.8695	0.2874	0.996	850.0974	0.7872	0.990	852.2601	0.2432	1.000
493.3919	0.6428	0.987	840.6983	0.4595	0.920	847.8700	0.2877	0.990	850.1671	0.8342	0.978	852.2606	0.2436	1.000
852.3296	0.2901	0.990	852.3997	0.3372	0.970	852.7409	0.5670	0.928	852.8108	0.6140	0.956	852.8804	0.6608	0.978
852.3301	0.2904	0.988	852.4002	0.3376	0.970	852.7414	0.5673	0.933	852.8113	0.6143	0.954	852.8809	0.6612	0.979

Observations for λ1550 Å

$JD_\odot$	Phase	Intensity	$JD_\odot$	Phase	Intensity	$JD_\odot$	Phase	Intensity	$JD_\odot$	Phase	Intensity	$JD_\odot$	Phase	Intensity
2440000+														
491.6532	0.4723	0.907	491.9322	0.6601	0.971	492.2796	0.8940	0.935	492.4193	0.9880	0.677	492.6276	0.1282	0.964
491.6538	0.4727	0.899	492.0706	0.7533	0.999	492.2802	0.8944	0.940	492.4886	0.0347	0.716	492.6282	0.1286	0.967
491.7923	0.5659	0.917	492.0712	0.7537	1.004	492.3491	0.9408	0.840	492.4892	0.0351	0.713	492.7055	0.1807	0.983
491.7929	0.5663	0.919	492.2101	0.8472	0.989	492.3497	0.9412	0.846	492.5666	0.0872	0.930	492.7061	0.1811	0.989
491.9316	0.6597	0.969	492.2107	0.8476	0.970	492.4187	0.9876	0.680	492.5672	0.0876	0.935	492.7756	0.2279	1.020

TABLE 1 - Continued

Observations for λ1550 Å, Continued

JD$_\odot$ 2440000+	Phase	Intensity	JD$_\odot$	Phase	Intensity	JD$_\odot$	Phase	Intensity	JD$_\odot$	Phase	Intensity	JD$_\odot$	Phase	Intensity
492.7762	0.2283	1.014	840.3507	0.2255	0.980	847.2419	0.8649	0.956	849.1910	0.1770	0.978	851.0025	0.3966	0.942
492.9060	0.3157	0.982	840.4180	0.2708	0.994	847.3143	0.9136	0.928	849.2635	0.2259	1.010	851.0029	0.3969	0.945
492.9066	0.3161	0.991	840.4188	0.2714	0.985	847.3149	0.9140	0.926	849.2639	0.2261	1.002	851.0035	0.3973	0.956
493.0458	0.4098	0.956	840.4434	0.2879	0.996	847.7283	0.1923	1.001	849.2645	0.2265	1.002	851.0695	0.4417	0.918
493.1230	0.4618	0.875	840.4442	0.2884	0.978	847.7293	0.1930	1.003	849.3336	0.2731	0.986	851.0699	0.4420	0.925
493.1234	0.4620	0.873	840.4456	0.2894	0.978	847.7981	0.2393	1.003	849.3340	0.2733	0.989	851.0705	0.4424	0.921
493.1845	0.5032	0.896	840.6966	0.4584	0.910	847.8686	0.2867	1.000	849.3346	0.2737	1.000	851.1436	0.4916	0.892
493.1851	0.5036	0.898	840.6974	0.4589	0.911	847.9371	0.3329	0.983	849.4034	0.3200	1.004	851.1440	0.4918	0.898
493.2540	0.5500	0.905	840.7664	0.5053	0.884	847.9375	0.3332	0.989	849.6783	0.5051	0.910	851.1446	0.4922	0.903
493.2546	0.5504	0.900	840.7671	0.5059	0.899	847.9381	0.3336	0.985	849.7462	0.5508	0.910	851.2086	0.5353	0.883
493.3241	0.5972	0.969	840.7685	0.5068	0.910	848.0067	0.3797	0.956	849.7466	0.5511	0.905	851.2090	0.5356	0.885
493.3252	0.5979	0.958	840.8359	0.5521	0.911	848.0070	0.3800	0.960	849.7472	0.5515	0.907	851.2096	0.5360	0.894
495.8306	0.2846	1.014	840.8367	0.5527	0.911	848.0076	0.3804	0.960	849.8166	0.5982	0.960	851.2830	0.5855	0.951
495.8312	0.2850	0.983	840.8381	0.5536	0.899	848.0764	0.4267	0.946	849.8170	0.5985	0.965	851.2834	0.5857	0.943
495.9004	0.3316	0.994	840.9056	0.5991	0.964	848.0767	0.4269	0.944	849.8866	0.6453	0.964	851.2840	0.5861	0.964
495.9010	0.3320	0.981	840.9064	0.5996	0.967	848.0774	0.4273	0.947	849.8872	0.6457	0.969	851.3533	0.6328	0.983
495.9699	0.3784	0.944	840.9078	0.6006	0.976	848.1459	0.4735	0.897	849.9557	0.6919	0.989	851.3537	0.6330	0.985
495.9705	0.3788	0.952	841.3937	0.9277	0.890	848.1463	0.4737	0.881	849.9561	0.6921	0.988	851.3543	0.6334	0.983
496.1091	0.4721	0.883	841.3951	0.9286	0.884	848.1469	0.4741	0.893	849.9567	0.6925	0.993	851.4236	0.6801	0.991
496.1098	0.4725	0.878	841.4632	0.9745	0.681	848.2155	0.5203	0.904	850.0255	0.7388	1.006	851.7637	0.9091	0.926
496.1787	0.5189	0.883	841.7410	0.1615	0.967	848.2158	0.5205	0.897	850.0258	0.7391	0.999	851.7648	0.9098	0.946
496.1793	0.5194	0.870	841.7418	0.1621	0.967	848.2164	0.5209	0.904	850.0264	0.7395	1.000	851.7654	0.9102	0.931
496.8053	0.9408	0.832	841.8102	0.2081	0.991	848.2852	0.5672	0.920	850.0950	0.7856	0.999	851.8343	0.9566	0.753
496.8059	0.9412	0.832	841.8116	0.2090	0.994	848.2855	0.5675	0.920	850.0954	0.7859	0.991	851.8347	0.9569	0.767
496.8748	0.9876	0.669	841.8130	0.2099	0.983	848.2861	0.5679	0.929	850.0960	0.7863	0.991	851.8353	0.9573	0.746
496.8755	0.9880	0.672	841.8803	0.2553	1.001	848.3593	0.6171	0.964	850.1645	0.8325	0.984	851.9041	0.0036	0.679
496.9444	0.0344	0.705	841.8811	0.2558	0.998	848.3596	0.6173	0.964	850.1649	0.8327	0.993	851.9044	0.0038	0.684
496.9450	0.0349	0.714	841.8825	0.2567	0.998	848.3602	0.6178	0.964	850.1655	0.8331	0.978	851.9050	0.0042	0.684
497.0929	0.1344	0.928	841.9500	0.3022	0.997	848.4254	0.6616	0.983	850.2342	0.8794	0.943	851.9769	0.0526	0.803
497.0935	0.1349	0.946	841.9508	0.3027	0.992	848.7038	0.8491	0.960	850.2346	0.8796	0.949	851.9772	0.0528	0.818
497.1625	0.1813	0.930	841.9522	0.3037	0.985	848.7718	0.8949	0.946	850.2352	0.8800	0.953	851.9778	0.0532	0.818
497.1631	0.1817	0.965	842.0196	0.3490	0.977	848.7722	0.8951	0.933	850.3089	0.9297	0.879	852.0444	0.0980	0.938
497.2229	0.2219	1.005	842.0204	0.3496	0.974	848.7728	0.8955	0.942	850.3083	0.9293	0.879	852.0448	0.0983	0.946
497.2235	0.2224	0.994	842.0217	0.3505	0.968	848.8421	0.9422	0.809	850.3156	0.9342	0.872	852.0454	0.0987	0.947
839.7219	0.8022	0.992	842.0899	0.3964	0.964	848.8425	0.9424	0.814	850.3782	0.9763	0.677	852.2582	0.2420	1.000
839.7227	0.8027	0.994	842.0913	0.3973	0.966	848.8431	0.9428	0.821	850.3786	0.9766	0.672	852.2592	0.2426	1.017
839.7914	0.8490	0.980	842.1588	0.4428	0.924	848.9142	0.9907	0.654	850.3792	0.9770	0.684	852.3278	0.2888	0.994
839.7922	0.8495	0.973	842.1596	0.4433	0.924	848.9146	0.9909	0.654	850.4493	0.0242	0.686	852.3281	0.2890	1.019
839.7936	0.8505	0.964	842.1610	0.4442	0.924	848.9152	0.9913	0.656	850.7207	0.2069	0.996	852.3287	0.2895	1.015
839.8610	0.8958	0.935	842.2291	0.4901	0.897	848.9812	0.0358	0.731	850.7211	0.2072	0.982	852.3984	0.3363	0.996
839.8618	0.8963	0.942	842.2305	0.4911	0.900	848.9816	0.0360	0.717	850.7217	0.2076	0.994	852.3988	0.3366	0.998
839.8632	0.8973	0.947	842.3032	0.5400	0.904	848.9822	0.0364	0.722	850.7894	0.2531	0.982	852.7383	0.5652	0.917
839.9300	0.9423	0.805	842.3035	0.5402	0.904	849.0511	0.0828	0.924	850.7903	0.2537	1.003	852.7394	0.5659	0.917
839.9308	0.9428	0.812	842.3040	0.5405	0.904	849.0514	0.0831	0.938	850.7909	0.2541	1.000	852.7400	0.5663	0.931
839.9322	0.9437	0.794	842.3054	0.5414	0.922	849.0521	0.0835	0.926	850.8600	0.3007	0.994	852.8089	0.6127	0.974
840.2788	0.1771	0.978	847.1714	0.8174	0.978	849.1204	0.1295	0.951	850.8604	0.3009	0.964	852.8093	0.6130	0.958
840.2796	0.1776	0.985	847.1718	0.8177	0.975	849.1208	0.1298	0.947	850.8610	0.3013	0.976	852.8099	0.6134	0.965
840.2810	0.1785	0.985	847.1724	0.8181	0.971	849.1214	0.1302	0.953	850.9295	0.3475	0.965	852.8785	0.6596	0.983
840.3485	0.2240	0.998	847.2410	0.8642	0.966	849.1900	0.1764	0.967	850.9299	0.3477	0.974	852.8788	0.6598	0.983
840.3493	0.2245	1.003	847.2413	0.8645	0.967	849.1903	0.1766	0.974	850.9305	0.3481	0.967	852.8795	0.6602	0.985

Observations for λ1430 Å

JD$_\odot$ 2440000+	Phase	Intensity	JD$_\odot$	Phase	Intensity	JD$_\odot$	Phase	Intensity	JD$_\odot$	Phase	Intensity	JD$_\odot$	Phase	Intensity
839.3753	0.5688	0.973	841.7425	0.1625	0.911	847.9387	0.3340	1.000	849.2651	0.2270	1.009	850.8616	0.3017	0.995
839.4031	0.5876	0.980	841.8122	0.2094	0.980	848.0083	0.3808	0.975	849.3352	0.2741	1.014	850.9311	0.3486	0.980
839.7236	0.8033	1.016	841.8817	0.2562	0.980	848.0780	0.4277	0.957	849.4040	0.3205	1.016	851.0041	0.3977	0.961
839.7927	0.8498	1.027	841.9514	0.3032	0.966	848.1475	0.4746	0.888	849.7478	0.5519	0.920	851.0711	0.4428	0.911
839.7931	0.8501	1.014	842.0210	0.3500	0.943	848.2171	0.5214	0.911	849.8183	0.5993	0.980	851.1452	0.4927	0.902
839.8624	0.8968	0.968	842.0905	0.3968	0.932	848.2868	0.5683	0.950	849.8878	0.6461	0.993	851.2102	0.5364	0.891
839.9314	0.9432	0.850	842.1602	0.4437	0.888	848.3609	0.6182	0.975	849.9573	0.6930	1.014	851.2847	0.5866	0.959
840.2802	0.1780	1.005	842.2298	0.4905	0.882	848.4260	0.6621	1.025	850.0271	0.7399	1.011	851.3549	0.6339	0.989
840.3499	0.2250	1.014	842.3046	0.5409	0.886	848.7735	0.8959	0.966	850.0966	0.7867	1.011	851.4243	0.6806	1.000
840.4195	0.2718	1.009	847.1730	0.8185	0.945	848.8437	0.9433	0.850	850.1661	0.8335	0.993	851.7660	0.9106	0.932
840.7678	0.5063	0.863	847.2426	0.8653	0.934	848.9158	0.9918	0.674	850.2359	0.8805	0.964	851.8359	0.9577	0.736
840.8373	0.5531	0.875	847.3156	0.9145	0.913	848.9828	0.0369	0.747	850.3096	0.9301	0.893	851.9057	0.0046	0.654
840.9070	0.6000	0.932	847.3851	0.9613	0.718	849.0527	0.0839	0.948	850.3798	0.9774	0.702	851.9785	0.0537	0.795
841.3943	0.9281	0.852	847.7988	0.2397	1.030	849.1220	0.1306	0.975	850.4499	0.0246	0.706	852.0460	0.0991	0.902
841.4639	0.9749	0.659	847.8692	0.2872	1.016	849.1916	0.1774	1.005	850.7915	0.2546	1.020	852.2598	0.2431	0.989
852.3293	0.2899	1.007										852.7406	0.5668	0.918
852.3994	0.3371	0.980										852.8105	0.6138	0.952
												852.8801	0.6606	0.966

TABLE 1 - Continued

Observations for λ1330 Å

$JD_{\odot}$ 2440000+	Phase	Intensity	$JD_{\odot}$	Phase	Intensity	$JD_{\odot}$	Phase	Intensity	$JD_{\odot}$	Phase	Intensity	$JD_{\odot}$	Phase	Intensity
839.3766	0.5697	0.280	841.9527	0.3040	0.985	848.1488	0.4754	0.885	849.8891	0.6470	0.969	851.2115	0.5373	0.892
839.4470	0.6171	0.977	842.0223	0.3508	0.954	848.2183	0.5222	0.908	849.9586	0.6938	1.000	851.2859	0.5874	0.962
839.7941	0.8508	0.977	842.0918	0.3977	0.954	848.2881	0.5692	0.923	850.0283	0.7408	0.992	851.3562	0.6347	0.992
839.8637	0.8976	0.946	842.1615	0.4446	0.892	848.3621	0.6190	0.962	850.0979	0.7876	0.985	851.4256	0.6814	1.000
839.9327	0.9441	0.816	842.2311	0.4914	0.885	848.7747	0.8968	0.931	850.1674	0.8344	0.977	851.7673	0.9115	0.916
840.2818	0.1791	0.977	842.3059	0.5418	0.916	848.8449	0.9440	0.816	850.2371	0.8813	0.946	851.8372	0.9586	0.739
840.3512	0.2258	0.985	847.1743	0.8194	0.969	848.9171	0.9926	0.672	850.3109	0.9310	0.885	851.9069	0.0055	0.667
840.4207	0.2726	0.992	847.2439	0.8662	0.954	848.9848	0.0382	0.739	850.3811	0.9783	0.710	851.9798	0.0545	0.831
840.7691	0.5072	0.892	847.3168	0.9153	0.916	849.0540	0.0848	0.931	850.4512	0.0255	0.716	852.0473	0.1000	0.939
840.8386	0.5540	0.908	847.3864	0.9621	0.724	849.1233	0.1315	0.954	850.7926	0.2553	1.008	852.2604	0.2435	1.054
840.9083	0.6009	0.939	847.8000	0.2406	0.992	849.1929	0.1783	0.985	850.8629	0.3026	0.985	852.3306	0.2907	1.023
841.3956	0.9290	0.854	847.8705	0.2880	1.000	849.2664	0.2278	1.008	850.9324	0.3494	0.969	852.4007	0.3379	1.000
841.4651	0.9758	0.716	847.9400	0.3348	0.985	849.3365	0.2750	1.015	851.0054	0.3986	0.969	852.8118	0.6147	0.962
841.8135	0.2103	0.985	848.0096	0.3817	0.962	849.4053	0.3213	0.985	851.0724	0.4437	0.916	852.8814	0.6615	0.985
841.8830	0.2571	0.992	848.0793	0.4286	0.939	849.8195	0.6002	0.969	851.1465	0.4935	0.908			

Note: The wavelengths used above to identify the light curves correspond to the photometer-filter combinations listed below. Details of the photometric system are given in Code, Houck, McNall, Bless, and Lillie (1970).

Wavelength	Photometer Number	Filter Number
4250 Å	Stellar 1	3
3320 Å	"	1
2980 Å	"	4
2460 Å	Stellar 3	2
1920 Å	"	1
1550 Å	Stellar 4	1
1430 Å	"	3
1330 Å	"	4

high dispersions, gave a velocity amplitude of $K_1 = 118$ km s^{-1}, derived from the presumably unblended helium lines, and a mass ratio of 0.572 from the shapes of the hydrogen lines near quadrature. These values lead to masses which are quite low for stars of the spectral types in MR Cyg, although reasonable masses would result if the mass ratio were reduced to 0.5. Clearly, further spectroscopic work would be useful.

Photometrically, MR Cyg is one of the more highly analyzed eclipsing binaries. A Russell-model solution was presented in the Hall-Hardie paper. In the Wilson and Devinney and in the Hill and Hutchings studies cited above, the Hardie light curves have been fit using light-curve synthesis techniques. The two resulting solutions differ somewhat in basic elements, the differences arising mainly from the difference in the assumed value of the mass ratio.

II. OBSERVATIONS OF VV ORIONIS

VV Orionis was observed in 1969 and in 1970 with the photometers and spectrum scanners aboard the OAO 2 spacecraft. The observed fluxes in eight bandpasses have been selected for presentation here. Table 1 lists the observations. The three quantities given are the heliocentric Julian date of the observation, the orbital phase of the observation, and the intensity—the observed flux, corrected for sky brightness, normalized to the flux at maximum light. At the end of table 1 the various photometer-filter combinations referred to by wavelength designations in the table and in the text are identified. The phases listed have been computed using the relation

$$JD_{\odot} = 2440470.1564\ JD_{\odot} + 1^{\mathrm{d}}.4853789E\,,$$

where E is the phase. This is practically the same ephemeris found by Schneller (1936) and used by Wood and by Huffer and Kopal. Obviously, the period has been quite constant over nearly half a century.

At the shorter wavelengths there was a rather large amount of scatter in the raw data—roughly 3 percent. For the three longest wavelengths, 4250, 3320, and 2980 Å, the scatter was comparable to that expected for good ground-based photometry. At wavelengths below 2980 Å the scatter was more severe, with segments of data shifted in intensity relative to other segments having about the same range of orbital phase. These shifts were not well correlated for the observations of the two shortest wavelength photometers, Stellar 3 and Stellar 4. One such shift seems to be associated with a passage of the instrument through the Earth's radiation belts. Some of the scatter may be due to atmospheric extinction since the star was observed close to the horizon. However, data taken a few minutes apart do not show the brightening with time expected if extinction were present. Normally in OAO 2 photometry observations may be normalized to a calibration source to take out changes in instrumental sensitivity. However, for Stellar 3 and Stellar 4 insufficient calibration source observations were made during the VV Ori observing runs. Only for Stellar 1 was the use of the calibration source possible. I have taken the scatter to be instrumental—extrinsic to the star—and have removed it from the observations at 2460, 1920, and 1550 Å through renormalization. The 1430 and 1330 Å observations have not been analyzed for scatter; they indicate the instrumental scatter of the raw data taken with Stellar 4. In the following analysis I have decided to combine the 3320 and the 2980 Å observations, calling the resulting light curve 3000 Å. The light curves for these two wavelengths are only slightly different in the sense that primary eclipse is slightly deeper at 2980 Å. Also, I have decided not to fit the 1430 and 1330 Å light curves since they are both similar to the 1550 Å light curve but are of lower quality.

Figure 1 is the energy distribution of VV Ori in the Balmer continuum. The solid line is the energy distribution for the primary as derived from scans obtained during the totality of secondary eclipse. The unit of flux used is 8.6×10^{-10} ergs cm^{-2} s^{-1} Å^{-1}. Two scans are plotted shortward of 1800 Å to indicate the observational scatter. This energy distribution was obtained from the scans using the OAO 2 absolute calibration in use as of 1974 June. It has been corrected for interstellar extinction corresponding to a color excess of $E(B - V) = 0.05$ mag using the mean extinction curve of Bless and Savage (1972). $E(B - V) = 0.05$ mag was inferred from the *UBV* colors and from the strength of the 2200 Å interstellar extinction feature in the spectrum. The triangles in figure 1 are the fluxes of the secondary plotted on a scale 100 times as sensitive as that used for the primary. These fluxes have been derived from the energy distribution of the primary and the ratio of surface brightness corresponding to the solution to be presented in table 2. At this dispersion I would classify the primary as B0 V to B1.5 V while the secondary is in the middle B range. The $(1700 - V)_0$ color of the primary, also corrected for $E(B - V) = 0.05$ mag, is -3.68 ± 0.1 mag. This corresponds to a spectral type of about B1 and to an effective temperature of

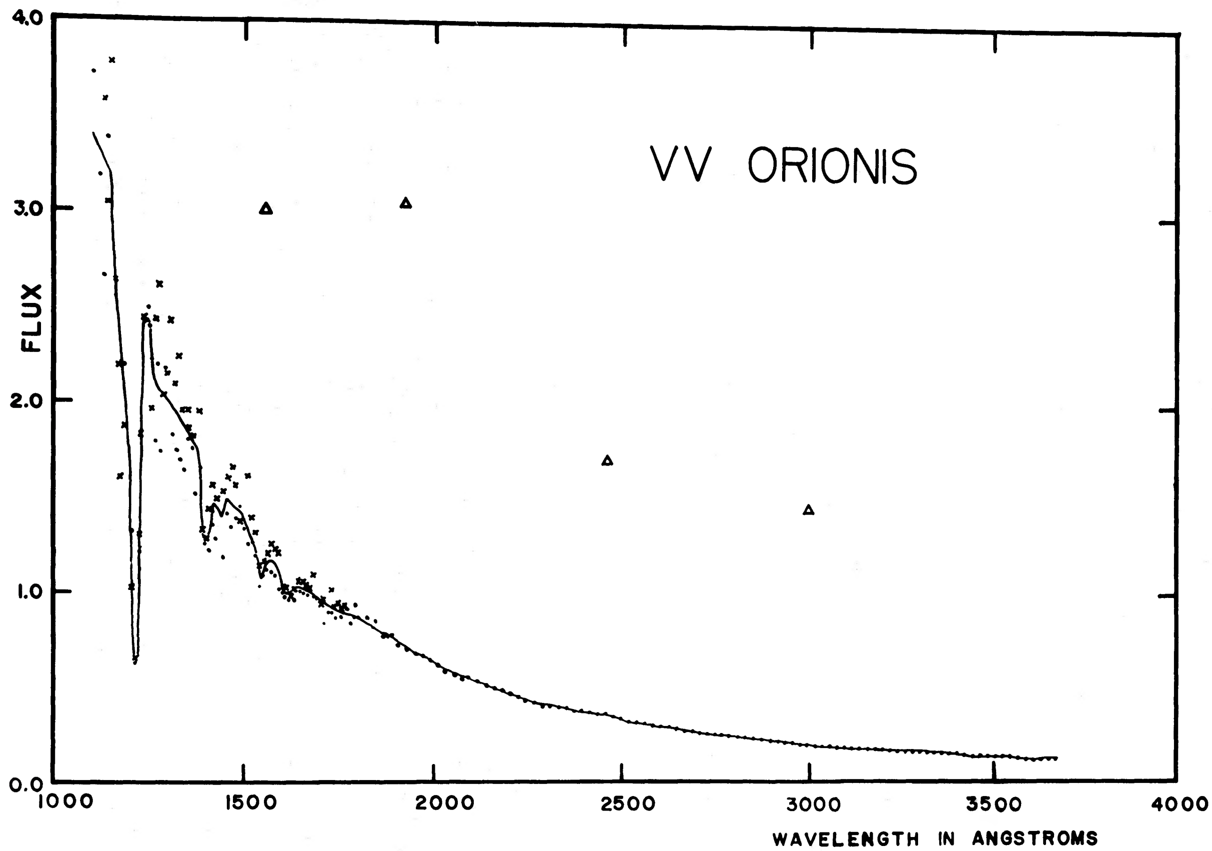

FIG. 1.—The ultraviolet spectrum of VV Ori. The flux per unit wavelength at the Earth, normalized to 1600 Å, is plotted against wavelength. The line is the energy distribution of the primary; two different scans are given as dots and crosses to indicate the observational uncertainties present. *Triangles*, the energy distribution of the secondary, plotted on a scale 100 times as sensitive as that used for the primary. The strong spectral feature near 1200 Å is the Lα line.

TABLE 2

ELEMENTS OF THE VV ORIONIS LIGHT-CURVE SOLUTION

A. WAVELENGTH-INDEPENDENT QUANTITIES

$i = 84.5° \pm 0.5°$
$r_1 = 0.3790 \pm 0.004$
$r_2 = 0.1745 \pm 0.004$
$k = r_2/r_1 = 0.460$
$q = m_2/m_1 = 0.458 \pm 0.05$
$g = 0.3\ (+0.1, -0.2)$
$T_1 = 21{,}000$ K (assumed for the light curve analysis)*

B. WAVELENGTH-DEPENDENT QUANTITIES

Wavelength (Å)	T_2 (K)	X_1	X_2 (assumed)
4250........	12,500 ± 200	0.30 ± 0.1	0.4
3000........	13,600*	0.55*	0.5
2460........	13,900	0.60	0.6
1920........	13,900	0.70	0.7
1550........	13,300	0.97	0.9

C. DERIVED ASTROPHYSICAL QUANTITIES

$T_1 = 25{,}000$ K $\pm$ 2000 K, $T_2 = 15{,}200$ K $\pm$ 500 K

	$\delta M_{bol} = 3.84$	
$M_1 = 9.3\ M_\odot$	$R_1 = 5.0\ R_\odot$	$\log L_1/L_\odot = 3.92$
$M_2 = 4.3\ M_\odot$	$R_2 = 2.3\ R_\odot$	$\log L_2/L_\odot = 2.39$

* See modifications in text.

25,400 ± 1500 K on the OAO effective temperature scale (Bless, private communication). (*1700 − V*) is defined as the magnitude difference corresponding to the ratio of the flux at 1700 Å to the flux in the *V* band of the *UBV* system and is a good temperature indicator for B stars.

III. METHOD OF LIGHT-CURVE ANALYSIS

The light curves presented in the last section have been fitted with theoretical light curves generated using the same geometrical model as used by Wilson and Devinney (1971) and by Hill and Hutchings (1973). The actual computational procedure used here was that developed by Lucy (1968) to model contact binaries, suitably modified to treat detached and semidetached components. This procedure, which mainly consists of finding intersections of a grid of "lines of sight" with a potential surface representing the binary component, has been extensively detailed by Rucinski (1973) for the common-envelope case. In the remainder of this section I shall discuss my modifications to this procedure.

In the case of detached components each star has its own value of the surface potential, reference temperature, reference gravity, and limb and gravity darkening laws. A star which is a detached or semidetached binary component has a maximum value of its radius in the direction toward its companion. Thus, any intersection of a line of sight with a binary component will take place in a sphere of this maximum radius centered on the component. These maximum radii for the two components become ρ_1 and ρ_2 in Rucinski's terminology. More logic is needed in this case of two potential surface than in the supercontact case to find all the visible elements of the surfaces, but this logic is straightforward.

The major difference between the light-curve synthesis computations used here and those done by others is in the calculation of surface brightness. In computing the intensity at some point on the surface of a component, the local effective temperature is given by the gravity darkening law

$$T = T_0(G/G_0)^{g/4}\,, \qquad (1)$$

where T_0 and G_0 are the reference temperature and gravity of the component in question, G is the local gravity, and g is a gravity exponent. This temperature implies a flux at the surface of the star, F_λ, found by interpolating in a table of F_λ versus T. This flux table may be taken from a model atmosphere grid or may be derived empirically from photometry and angular diameters of stars with known effective temperatures. In practice I use the theoretical fluxes tabulated by Kurucz, Peytremann, and Avrett (1972) for all spectral regions except the *U* band of the *UBV* system. The agreement between these theoretical fluxes and the empirical fluxes assembled for stars in the OAO effective temperature study is excellent to within a multiplicative factor for *B* and *V* but is quite poor for *U*. Also, this grid of models seems to fit observed energy distributions well in the ultraviolet wavelengths covered by our observations. For the *U* band I use a relation formed from the observed *U* fluxes and observed temperatures.

Once the emergent flux is known, the intensity in the line of sight is given by

$$I(\mu) = \frac{F_\lambda}{\pi(1 - x/3)}\cdot(1 - x + x\mu)\,, \qquad (2)$$

where a cosine law of limb darkening has been assumed. Here, x is the limb darkening coefficient and μ is the cosine of the angle between the line of sight and the surface normal.

In this study the physical interaction of the reflection effect is taken to be absorption and reemission of all incident radiation. In this approximation the reflection effect may be further assumed to be a heating up of the surface—which may be included in the computation of local effective temperature through a factor R:

$$T = RT_0(G/G_0)^{g/4}\,. \qquad (3)$$

In practice I assume R is a function of l only, l being the cosine of the angle between the local radius and the substellar point. R is found from a table of R versus l with R computed for the point in the orbital plane corresponding to each l, l running from 1.0 to −1.0 in steps of 0.10. R is given by the relation

$$R(l) = [1 + F_{in}^{bol}(l)/F_0^{bol}(l)]^{0.25}\,, \qquad (4)$$

where F_{in}^{bol} is the bolometric flux received from the companion, found through a numerical integration over the companion, and F_0^{bol} is the local bolometric flux at l with no incident radiation.

Rucinski (1970) has studied the wavelength dependence of reflection effect for one particular system. His calculations showed that the energy distribution of the reradiated flux is different from that of the incident flux and from that of the unilluminated atmosphere. It also differs from the flux surplus of a normal atmosphere of the same total emergent flux as the illuminated atmosphere over the illuminated atmosphere. These results are really not unpredictable and may be generalized. The most important point here is that a large part of the incident flux is deposited in the first optical depth or so of the irradiated atmosphere. To a low order of approximation this may be considered as the heating up of an optically thin, isothermal slab. This slab will radiate intensity at some wavelength proportional to the Planck function for the slab temperature and proportional to the monochromatic optical thickness of the slab. Such a 12,000 K slab, corresponding to a late B star, should radiate strongest just shortward of the Balmer jump because the opacity and Planck function are both high there; it will radiate very little at 1000 Å where the opacity and Planck function are both low. Similarly, appropriately irradiated stars like the Sun should reradiate strongest in the near-infrared where the Planck function is high and the H^- opacity peaks.

Rucinski has defined a monochromatic albedo, A_λ, which is just the flux surplus of the illuminated atmosphere over the unilluminated atmosphere divided by the incident flux. A more directly observable quantity is the ratio of the actual flux surplus to the flux surplus if the atmosphere radiated as a normal atmosphere of the same emergent bolometric flux. I will call this quantity A_λ'.

IV. SOLUTION OF THE VV ORIONIS LIGHT CURVES

The VV Ori light-curve solution was obtained by varying the appropriate elements by trial and error to obtain a fit to the light curves; a formal least-squares corrections procedure was not used. However, the quantitative knowledge of how changing a given element changes the light curve guided all variations of the elements. The elements g and q depend on the simultaneous fit of all five light curves, while r_1, r_2, and i depend mostly on the fit of the best light curve, 4250 Å. The nature of the VV Ori light variation made possible a highly reliable solution. Both the radii and the limb and gravity darkening of the primary are especially determinate. Out-of-eclipse (tidal) distortion of the light curve is highly dependent on the mass ratio and on the radius and gravity darkening of the primary. The wavelength dependence of this out-of-eclipse distortion is determined primarily by gravity darkening of the primary. Primary eclipse depth is most highly dependent on the ratio of radii, while the phases of internal and external contact provide further restrictions on the radii. The shape of the bottom of primary eclipse is determined chiefly by the limb darkening of the primary. The brightness distribution on the eclipsed face of the secondary, however, is influenced to a great extent by reflection effect, and little of the tidal distortion of the light curve is contributed by the secondary. Hence, the limb and gravity darkening of the secondary are not really determinable.

The best of the five light curves, 4250 Å, was fitted for an assumed value of the gravity exponent. Initially, $g = 1$ was used, as theoretically expected for stars with radiative envelopes. An excellent 4250 Å fit was

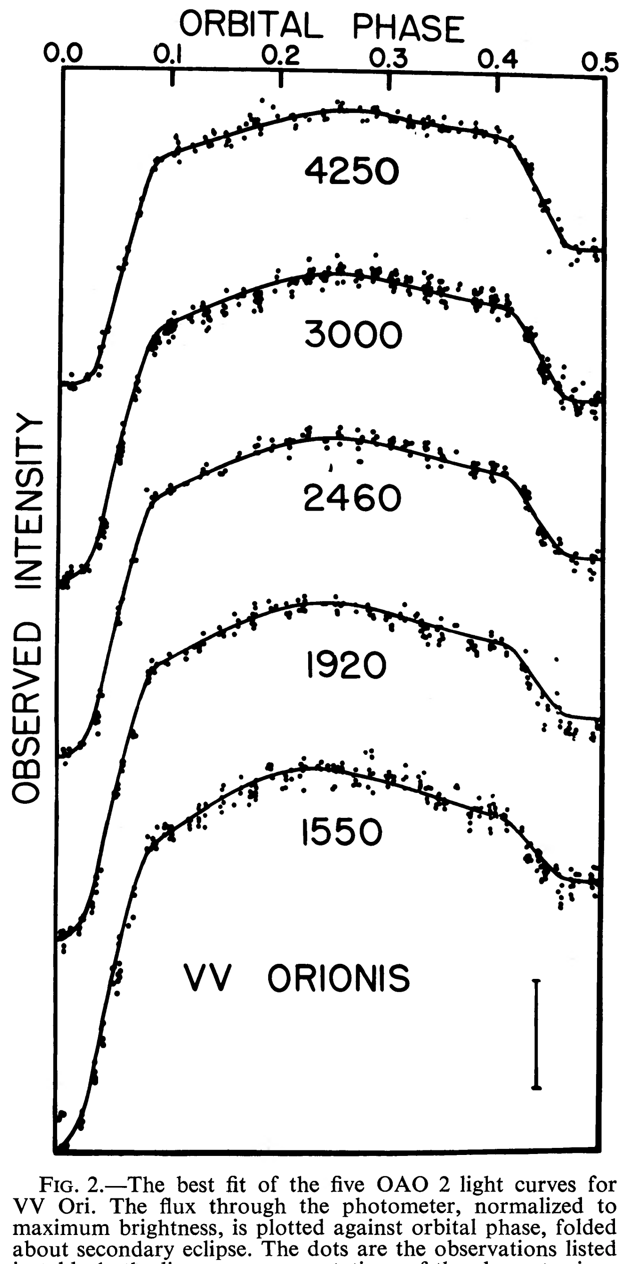

FIG. 2.—The best fit of the five OAO 2 light curves for VV Ori. The flux through the photometer, normalized to maximum brightness, is plotted against orbital phase, folded about secondary eclipse. The dots are the observations listed in table 1; the lines are representations of the elements given in table 2. Each light curve is identified by a wavelength as in table 1. The bar in the lower right corner has a length of 0.1 light unit.

TABLE 3

GRAVITY-DARKENED SOLUTION FOR VV ORIONIS

A. WAVELENGTH-INDEPENDENT QUANTITIES

$i = 84^\circ.25 \pm 0^\circ.5$
$r_1 = 0.3670 \pm 0.004$
$r_2 = 0.1735 \pm 0.004$
$q = 0.45$
$g = 1.0$ (assumed)
$T_1 = 21{,}000$ K
$T_2 = 11{,}800$ K

B. WAVELENGTH-DEPENDENT QUANTITIES

Wavelength (Å)	X_1	X_2 (assumed)
4250............	0.20 ± 0.1	0.4
2460............	0.55 ± 0.2	0.6
1550...........	0.80 ± 0.2	0.9

obtained, but the corresponding far-ultraviolet light curves were much too highly distorted. The wavelength variation of tidal distortion is fitted best with $g = 0.3$. The complete solution for this value is given in table 2, and the representation of it is plotted along with the observations in figure 2. For comparison the best $g = 1$ solution is given in table 3 and represented in figure 3. The radii listed are the side radii of the two components—the radii corresponding to the direction 90° from both the pole and substellar point. They correspond to r(side) and to E in the terminology of Wilson and Devinney and of Hill and Hutchings, respectively. The uncertainties given in table 2 indicate the range of each element over which I think reasonable solution of this set of light curves is possible. Also listed in table 2 is the effective temperature of the secondary, as deduced from each of the five light curves. The effective temperature of the primary was assumed to be 21,000 K for all wavelengths. The differences in secondary temperature should be interpreted as deviation of the energy distributions of the actual stars from the energy distributions representing them in the light-curve calculations. The main effect is in the 4250 Å band, indicating too large a Balmer jump for the secondary in the calculations. This may be corrected by increasing the primary temperature to 25,000 ± 1500 K and the secondary temperature to 15,200 K. Experience with calculations for this system shows that this change in temperature will change the calculated light curves only very slightly. This temperature determination may also be considered a fundamental determination of the temperatures of the two stars. VV Ori is known spectroscopically to have a third component which must have been included in the OAO photometry. The work of Beltrami and Galeotti (1970) implies a third body contributing about 2 percent of the light in the blue. Since the eclipses are shallow, third light at this level has very little effect on the light curve. For instance, its effect on the out-of-eclipse light is much less than the observational scatter. Including this amount of third light in the eclipse solution will result in a larger ratio of radii and a small increase in the secondary temperature, something on the order of less than 100 K. The third section of table 2 gives properties of the system derived from combining Beltrami and Galeotti's velocity amplitude for the primary with the light-curve solution.

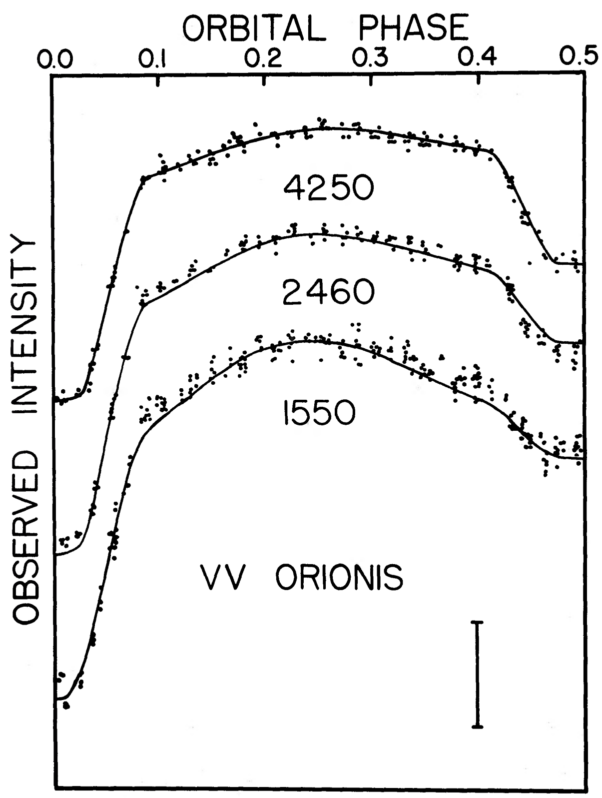

FIG. 3.—The representation of the fully gravity-darkened solution. The observations at three wavelengths are plotted as in fig. 2. The lines are representations of the elements given in table 3. The bar in the lower right corner has a length of 0.1 light unit.

It is of interest to look at some of the discrepancies in the fits. Referring to figure 2, the fits are excellent for 4250 Å and for 2460 Å. The 3000 Å light curve is quite systematically misfit. It was computed for the same assumed reflection effect used to compute the other four light curves, namely, that the albedo of the secondary, A_λ', is unity. Figure 2 shows that this is detectably wrong at 3000 Å. This albedo as determined from the deviation of the fit is $A_\lambda' = 1.5 \pm 0.2$. This is a reflection–flux-weighted mean albedo. It should be noted that A_λ' at the other four wavelengths is close to unity, rather than becoming lower at 1550 Å. For 3000 Å, T_2 and x_1 are also systematically wrong because of the albedo assumption. T_2 should be reduced slightly, while the x_1 listed in table 2 should be decreased by 0.07 as a result of changing the reflection effect. Two other discrepancies which should be noted are the poor fit of secondary eclipse depth at 1920 Å and the fact that the computed primary at 1550 Å is too narrow.

The above solution is well determined if the model used is applicable. A major question as to applicability concerns the possibility that the radius of the primary varies with wavelength. The 1550 Å fit, for instance, could be improved by using a larger r_1. A wavelength-dependent radius implies either an extended atmosphere or that the wrong limb darkening law was assumed. The spectrum of the primary, given in figure 1, is that of a very early B star, a *dwarf* as deduced from the strengths of the gravity-dependent C IV and Si IV lines. The wavelength dependence of the limb darkening coefficient and shape of the continuum are about what are expected for a plane-parallel atmosphere of the appropriate temperature and gravity. These atmospheres are not expected to be extended; their limb darkening is expected to be reasonably well represented by a cosine law. Considering the neutral hydrogen continuum opacity alone, such an atmosphere should look *smaller* at 1550 Å than at 2460 Å if it is extended.

V. DISCUSSION OF MR CYGNI

If the gravity darkening result for VV Ori is generally correct for early B stars, it should be possible to fit MR Cyg using this same gravity darkening. Compared with VV Ori, the light curves for MR Cyg are much more dependent on the reflection effect since the stars have a larger ratio of radii and a similar temperature difference. Also, the mass ratio is not well known spectroscopically. It was marginally possible to fit Hardie's *UBV* observations with the elements listed in table 4 and represented in figure 4. These fits are fairly good, suffering from deviations similar to those of the solutions of Wilson and Devinney and of Hill and Hutchings. Fitting the MR Cyg light curves for $g < 1$ is a matter of making r_1 and q large enough to fit the tidal distortion. The value of r_1 given in table 4 is about as big as it can get before running into the constraints of the eclipse depths and external tangency. This solution may well have been pushed to too large a value of q, as will be discussed in the next section. However, contrary to the conclusion of Wilson and Devinney, complete gravity darkening is not required to fit the visual light curve.

TABLE 4

ELEMENTS OF THE MR CYGNI LIGHT-CURVE SOLUTION

A. WAVELENGTH-INDEPENDENT QUANTITIES

$i = 85\overset{\circ}{.}0$
$r_1 = 0.368$
$r_2 = 0.280$
$q = 0.83$
$g = 0.3$ (assumed)
$T_1 = 18{,}400$ K
$T_2 = 11{,}050$ K
$\delta M_{\rm bol} = 2.81$

B. WAVELENGTH-DEPENDENT QUANTITIES

Wavelength	X_1	X_2 (assumed)	A_λ'
V..........	0.55 (assumed)	0.0	1.0 ± 0.2
B..........	0.65 ± 0.1	0.0	1.0
U..........	0.65 ± 0.1	0.0	1.33

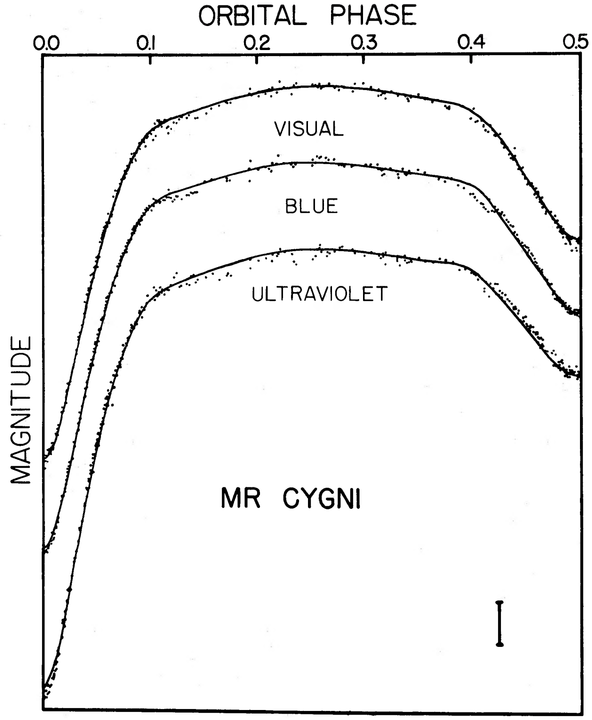

FIG. 4.—The $g = 0.3$ solution for MR Cyg. The elements of table 4 are represented by the lines. The dots are the *UBV* observations of Hardie. The bar in the lower right corner has a length of 0.1 mag.

An important result of this MR Cyg study is the opportunity to critically compare light curves computed by several light-curve synthesis schemes. No uncertainties of elements have been given in table 4. Such uncertainties are best appreciated by intercomparing this solution with those of Wilson and Devinney and of Hill and Hutchings. Light-curve synthesis can be used to derive highly accurate solutions of binary-star light curves. However, it is imperative that surface brightness be handled correctly in this procedure in order to avoid systematic errors. The details of surface brightness determine the out-of-eclipse light curve to a substantial degree. Gravity darkening enters the surface brightness through the slope of the flux-temperature relation. For this reason, fitting a tidally distorted light curve by using different flux-temperature relations will result in systematically different elements. My representation of the Wilson and Devinney V elements, calculated using blackbody atmospheres and $T_2 = 12{,}200$ K, was quite close to their published representation. This is an encouraging indication of consistency between the geometrical calculations of two rather different light-curve synthesis programs. However, a representation of these same elements using the Kurucz *et al.* (1972) fluxes was noticeably less distorted tidally. This is to be expected since the blackbody intensities vary faster with temperature than the atmosphere fluxes do. Also, my representations of Hill and Hutchings's elements were somewhat less distorted than their published representations. The use of an empirically correct flux table as done here has the advantages of both accuracy and simplicity. It is about as simple as using a blackbody law. Furthermore, it makes it possible to study wavelengths for which blackbodies or simple atmospheres computed locally are totally inadequate. Finally, it makes it possible to use an actual representative effective temperature of each star in the light curve calculations; no temperature calibration is necessary.

VI. DISCUSSION OF RESULTS

Both of these stars are interesting from the points of view of stellar atmospheres and stellar evolution. The well-determined limb darkening of the VV Ori primary is quite close to that expected from model atmospheres with opacity not dominated by electron scattering (Grygar 1965). The wavelength dependence of the limb darkening for MR Cyg is about that theoretically expected, although the values found are probably systematically too high. The gravity darkening result for VV Ori was completely unexpected. Previous studies in the optical (Kopal 1968) and even in the Balmer continuum (Eaton and Ward 1973) indicated that full gravity darkening is consistent with observed light curves. Gravity darkening for hot stars is very difficult to determine from optical observations alone. Figures 2 and 3 indicate that it would not be possible to determine g from blue observations of VV Ori alone, even with a highly accurate spectroscopic mass ratio. The main effect of gravity darkening is to increase the tidal distortion of the light curve. Since this increase is greater at wavelengths at which flux varies more rapidly with effective temperature, it is important to observe in the ultraviolet as well as in the optical for B stars. Tidal distortion is also dependent on limb darkening, and it would be possible to rescue gravity darkening by reducing the wavelength variation of limb darkening. However, for VV Ori, limb darkening is highly restricted by the eclipse depths and shapes. The values of x_1 listed in table 2 are determined mainly from eclipse *depths*, but they fit the *shapes* of the complete transit phases of primary eclipse as well. Limb darkening must be close to unity for 1550, 1430, and 1330 Å from eclipse shapes alone; at 4250 Å, x_1 can be no larger than a few tenths. Bless (private communication) has looked for gravity darkening effects in the far-ultraviolet observations of rapidly rotating stars, with null results. Because of inclination, distance modulus, and extinction effects, it is at least an order of magnitude harder to detect gravity darkening in single stars than in binaries, but his result is at least indicative. A value of $g < 1$ has implications for binary components near their Roche lobes, since there will be more flux passing through the stellar surface near the inner Lagrangian point than in the $g = 1$ case. In some cases this flux is expected to extend the atmosphere in this region of low gravity, leading to a bulge on the star which could complicate its light curve.

For MR Cyg it should be possible to determine g from optical observations provided the mass ratio is known from spectroscopy. Considering the source of the work and the dispersions used, the Hill and Hutchings radial velocity study is very compelling. Unfortunately, it leads to rather low masses using the observed mass ratio $q = 0.57$ and to even worse masses using the mass ratio $q = 0.62$ adopted for their light curve study. The solution presented here indicates that low gravity darkening is a possibility for MR Cyg, but this requires the mass ratio to be much closer to unity than observed by Hill and Hutchings or than expected from the zero-age main sequence (ZAMS) mass-luminosity relation. Morton and Adams (1968) have tabulated the observationally determined ZAMS. For the temperatures and luminosity ratio of table 4 the secondary lies 0.5 mag above the main sequence if the primary lies on the main sequence. Assuming the secondary is still contracting toward the main sequence, it is close enough to the ZAMS that it should join it with little change in luminosity. Thus, it should presently obey the ZAMS mass-luminosity relation, implying a mass ratio of about 0.5. This low value of $q = 0.5$ combined with the velocity amplitude of $K_1 = 118 \text{ km s}^{-1}$ leads to low but plausible masses of 5.1 and 2.5 $M_\odot$ for the components as well as implying a high value of the gravity exponent in the context of the Roche model. A more interesting hypothesis is that the Roche model is inadequate for this system, as has been suggested by Hill and Hutchings. A 2000 Å light curve would be instrumental in confronting this hypothesis by observationally fixing the gravity darkening and temperatures of the stars, allowing attention to be focused on *gravitational* distortion. VV Ori seems to be a reasonably normal main-sequence pair. When plotted on the observational ZAMS, the primary lies a little above the main sequence while the secondary lies slightly below.

I wish to acknowledge several helpful discussions with R. C. Bless of the University of Wisconsin and with E. W. Weis at the University of Florida. The use of the physics library at the University of Florida where this paper was written is also appreciated, as were J. P. Cassinelli's comments on the manuscript. This research was supported in part by NASA contract NAS5-1348 and by the Wisconsin Alumni Research Foundation.

REFERENCES

Beltrami, G., and Galeotti, P. 1970, *Mem. Soc. Astr. Italiana, Ser. 3*, **41**, 167.
Bless, R. C., and Savage, B. D. 1972, *Ap. J.*, **171**, 293.
Code, A. D., Houck, T. E., McNall, J. F., Bless, R. C., and Lillie, C. F. 1970, *Ap. J.*, **161**, 377.
Daniel, Z. 1915, *Pub. Allegheny Obs.*, **3**, 179.
Eaton, J. A., and Ward, D. H. 1973, *Ap. J.*, **185**, 921.
Grygar, J. 1965, *Bull. Astr. Inst. Czechoslovakia*, **16**, 195.
Hall, D. S., and Hardie, R. H. 1969, *Pub. A.S.P.*, **81**, 754.
Harper, W. E., Pearce, J. A., Petrie, R. M., and McKellar, A. 1935, *J.R.A.S. Canada*, **29**, 411.
Hill, G., and Hutchings, J. B. 1973, *Ap. and Space Sci.*, **20**, 123.

Huffer, C. M., and Kopal, Z. 1951, *Ap. J.*, **114**, 297.
———. 1952, *A.J.*, **57**, 160.
Kopal, Z. 1968, *Ap. and Space Sci.*, **2**, 166.
Kurucz, R. L., Peytremann, E., and Avrett, E. H. 1972, *Blanketed Model Atmospheres for Early-Type Stars* (Washington: Smithsonian Institution Press).
Lucy, L. B. 1968, *Ap. J.*, **153**, 877.
Morton, D. C., and Adams, T. F. 1968, *Ap. J.*, **151**, 611.
Rucinski, S. M. 1970, *Acta Astr.*, **20**, 327.
———. 1973, *ibid.*, **23**, 79.
Schneller, H. 1936, *Kleine Ver. Berlin-Babelsberg*, No. 17.
Struve, O., and Luyten, W. J. 1949, *Ap. J.*, **110**, 160.
Wilson, R. E., and Devinney, E. J. 1971, *Ap. J.*, **166**, 605.
Wood, F. B. 1946, *Contr. Princeton Obs.*, **21**, 25.

JOEL A. EATON: Washburn Observatory, University of Wisconsin, 475 North Charter St., Madison, WI 53706